Published in final edited form as:
Nat Cell Biol. 2013 March ; 15(3): 284–294. doi:10.1038/ncb2690.

miR-126 and miR-126* repress recruitment of mesenchymal stem cells and inflammatory monocytes to inhibit breast cancer metastasis

Yun Zhang[1,7], **Pengyuan Yang**[1,2,7], **Tao Sun**[1], **Dong Li**[2,8], **Xin Xu**[1], **Yaocheng Rui**[2], **Chaoran Li**[3], **Mengyang Chong**[1], **Toni Ibrahim**[4], **Laura Mercatali**[4], **Dino Amadori**[4], **Xincheng Lu**[5], **Dong Xie**[6], **Qi-Jing Li**[3,9], and **Xiao-Fan Wang**[1,9]

[1]Department of Pharmacology and Cancer Biology, Duke University Medical Center, Durham, North Carolina 27710, USA

[2]Department of Pharmacology, Second Military Medical University, Shanghai 200433, China

[3]Department of Immunology, Duke University Medical Center, Durham, North Carolina 27710, USA

[4]Osteoncology and Rare Tumors Center, IRCCS Istituto Scientifico Romagnolo per lo Studio e la Cura dei Tumori (I.R.S.T.), Meldola 47014, Italy

[5]Institute of Genomic Medicine, Wenzhou Medical College, Wenzhou, Zhejiang 325027, China

[6]Laboratory of Molecular Oncology, Institute for Nutritional Sciences, Shanghai Institutes of Biological Sciences, Shanghai 200031, China

Abstract

The tumour stroma is an active participant during cancer progression. Stromal cells promote tumour progression and metastasis through multiple mechanisms including enhancing tumour invasiveness and angiogenesis, and suppressing immune surveillance. We report here that miR-126/miR-126*, a microRNA pair derived from a single precursor, independently suppress the sequential recruitment of mesenchymal stem cells and inflammatory monocytes into the tumour stroma to inhibit lung metastasis by breast tumour cells in a mouse xenograft model. miR-126/miR-126* directly inhibit stromal cell-derived factor-1 alpha (Sdf-1α) expression, and indirectly suppress the expression of chemokine (C–C motif) ligand 2 (Ccl2) by cancer cells in an Sdf-1α-dependent manner. miR-126/miR-126* expression is downregulated in cancer cells by promoter methylation of their host gene *Egfl7*. These findings determine how this microRNA pair alters the composition of the primary tumour microenvironment to favour breast cancer metastasis, and

[9]Correspondence should be addressed to Q-J.L. or X-F.W. (qi-jing.li@duke.edu or xiao.fan.wang@duke.edu).
[7]These authors contributed equally to this work
[8]Present address: Department of Oncology, Chengdu Military General Hospital, Chengdu, Sichuan 610083, China

Note: Supplementary Information is available in the online version of the paper

AUTHOR CONTRIBUTIONS

Y.Z., P.Y. and X.W. designed the research; Y.Z. and P.Y. performed most experiments and analysed the results; T.S., X.X., C.L. and M.C. provided further technical assistance; D-J.L. and Y.R. provided technical assistance in luciferase reporter assay and MSCs isolation; T.I., L.M., D.A. and X.L. provided clinical samples and associated analyses; Y.Z. and X-F.W. wrote the manuscript; P.Y., D.X. and Q-J.L. edited the manuscript.

COMPETING FINANCIAL INTERESTS

The authors declare no competing financial interests.

Accession codes. Primary accessions. Gene Expression Omnibus GSE42884, GSE42885
Referenced accessions. Gene Expression Omnibus GSE3494

demonstrate a correlation between miR-126/126* downregulation and poor metastasis-free survival of breast cancer patients.

Metastasis accounts for about 90% of the deaths of cancer patients[1–3]. Tumour-associated stromal cells are thought to play a critical role in functionally defining the tumour microenvironment that influences cancer progression, metastasis and recurrence following treatment[4,5]. The metastatic abilities of cancer cells were shown to be enhanced by their interactions with tumour-infiltrating stromal cells, such as endothelial progenitor cells (EPCs) and mesenchymal stem cells[6–8] (MSCs), demonstrating that the metastatic phenotype develops not only due to cell-autonomous changes but also due to influences exerted by non-malignant cells inside the tumour microenvironment[5,9,10].

MicroRNAs, a class of 21–23-nucleotide non-coding RNAs that suppress the expression of their target messenger RNAs (ref. 11), participate in many steps of cancer progression, including metastasis[12,13]. In breast cancer, the expression profile of several microRNAs was found to associate with metastasis and poor disease prognosis[14–16]. Among them, miR-126 was shown to inhibit angiogenesis and lung metastatic colonization by the human breast cancer MDA-MB-231 cells[17]. Here we report that the miR-126/miR-126* microRNA pair act through a different mechanism to promote cancer cell invasion and metastasis, as downregulation of their expression leads to an increased level of production of Sdf-1α (also known as Cxcl12) and Ccl2, two chemokines involved in the recruitment of two different types of stromal cell to the primary tumour microenvironment.

RESULTS

miR-126/126* are metastasis suppressors in breast cancer

To investigate the role of microRNAs in the interactions between cancer cells and their microenvironment, we performed an unbiased screen of 242 microRNAs using a series of human breast cancer cell lines derived from the same breast epithelial cell line MCF10A and identified 17 microRNAs that exhibited significant expression changes correlated with the metastatic potential of these cells (Fig. 1a). Among the downregulated microRNAs, miR-126 (miRBase accession no. MIMAT0000445) was previously shown to correlate with poor overall metastasis-free survival in breast cancer patients[16], and to suppress metastasis through targeting several genes important for angiogenesis[17]. miR-126* (miRBase accession no. MIMAT0000444), the partner to miR-126 that is derived from the same transcript, had a similar expression pattern (Fig. 1a,b). Consistent with those previous reports[16,17], analysis of breast cancer patient clinical samples revealed that miR-126 is downregulated in metastatic tissues compared with primary tumour specimens, with miR-126* exhibiting a similar pattern (Fig. 1c). Although the miR-126/miR-126* detected in the clinical samples could be of tumour and/or stromal cell origin, together the data indicate that these two microRNAs are potential suppressors of the metastatic process. To gain further insight into the biological function of miR-126/miR-126* in breast cancer progression, we used the well-characterized 4T1 murine mammary tumour cells and their syngenic BALB/c mouse host as the model system, because the behaviour of 4T1 cells highly resembles metastatic breast cancer in humans and they express miR-126/miR-126* at similar levelps to the metastatic M-IV cells (Fig. 1b).

Employing a retroviral delivery system, we generated 4T1 cell populations that harbour a vector control (4T1-C) or ectopically produce pri-miR-126, which generates both miR-126 and miR-126* (4T1-M; Supplementary Fig. S1a,b). In contrast to previous reports that miR-126 overexpression could affect cell proliferation or migration[16,18], these two cell populations exhibited little difference in proliferation and migration *in vitro* (Supplementary

Fig. S1c,d). Following an established procedure[19,20] (Fig. 1d), we implanted luciferase-labelled 4T1-C or 4T1-M cells into the mammary fat pad of female BALB/c mice. At 10 days post-inoculation, primary tumours were surgically removed with no residual luciferase signal detected in the animals (Fig. 1f). Consistent with their comparable *in vitro* proliferation rates, these two cell populations formed primary tumours with a similar size and weight (Fig. 1e). Immunostaining of tumour sections for the Ki-67 proliferation marker revealed that ectopic expression of pri-miR-126 had little effect on tumour cell proliferation *in vivo* (Supplementary Fig. S1e,f). In contrast, pri-miR-126 ectopic expression significantly suppressed the formation of lung metastases at 7 and 14 days after the surgical removal of the primary tumours (Fig. 1f,g). We next generated a 4T1-derived cell line stably expressing microRNA sponges targeting both miR-126 and miR-126* (4T1-SP-both). Although the expression levels of miR-126/126* are relatively low in 4T1 cells (Fig. 1b), suppressing these microRNAs significantly increased the ability of these cells to metastasize to the lung (Supplementary Fig. S2).

Sdf-1α/Cxcl12 is a direct target of both miR-126 and miR-126*

To explore how these microRNAs suppress metastasis in our system, we inoculated 4T1-C or 4T1-M cells into BALB/c mice through tail-vein injection and counted metastatic nodules on the lungs two weeks later. No difference in the number or the size of tumour nodules was observed between the two groups in this experimental setting (Fig. 2a,b), in sharp contrast to the reported phenotype using the model of MDA-MB-231 cells and SCID mice[17]. Examination of the expression levels of *IGFBP2, PITPNC1* and *MERTK*, three miR-126 targets identified in the earlier report[17], showed that they were affected differently in 4T1-C and 4T1-M cells when compared with MDA-MB-231 cells (Supplementary Fig. S3). Thus, in our model, pri-miR-126 may influence the metastatic process through a different mechanism from the reported one, perhaps at the primary tumour site before cancer cells intravasate into the circulation, and through targeting the expression of secreted proteins, such as cytokines and chemokines. Considering the possibility that the production of cytokines/chemokines may depend on the interactions among different cell types within the tumour mass, we inoculated GFP-labelled 4T1-C or 4T1-M cells into the fat pad of BALB/c mice and collected the primary tumours 10 days later to isolate GFP^+ cancer cells. We then analysed the expression profile of 95 cytokines/chemokines and their receptors at the mRNA level (Fig. 2c) and identified five cytokine/chemokines to exhibit more than a twofold change in expression level with a significant *P* value ($P < 0.5$; Fig. 2d). We also employed several commonly used bioinformatic algorithms[21,22] to identify potential targets of miR-126/miR-126* among the 95 genes and found that only the 3′-UTR of *Sdf-1α/Cxcl12* contained putative binding sites for both microRNAs (Fig. 2e). We cloned the human and mouse *Sdf-1α* 3′-UTRs into a luciferase reporter plasmid and co-transfected either construct with pri-miR-126 into HEK293T cells. As shown in Fig. 2e,f, only the wild-type version of the reporters was significantly suppressed by pri-miR-126 in a dose-dependent manner, implicating *Sdf-1α* as a direct target of miR-126 and/or miR-126* in both human and mouse.

In most reported cases, only the strand with a weaker 5′-terminal thermo-stability, termed the guiding strand of the microRNA duplex, can be incorporated into the RNA-induced silencing complex (RISC) composed mainly of Ago proteins after pri-microRNAs are processed by Drosha and Dicer to generate the microRNA duplex, whereas the star strand of the duplex is degraded rapidly after strand-loading[23]. By determining the copy number of miR-126 and miR-126* per cell by quantitative real-time PCR (rtPCR), we found both microRNAs to be present in similar numbers in M-II and 4T1 cells (Fig. 3a,b), suggesting no obvious strand bias between them during RISC loading and protection. We then performed RNA chromatin immunoprecipitation analysis on 4T1-M cells (Fig. 3c,d) and

determined the relative efficiency of RISC loading for several microRNA pairs through quantitative rtPCR. For miR-21/miR-21★ and miR-9/miR-9★, which served as controls, only the designated guiding strand was incorporated into RISC, indicating that 4T1 cells are not exempt from the general rule of miRNA strand selection. In sharp contrast, miR-126* was incorporated into RISC with a significantly higher efficiency when compared with the star strand of the two control miRNAs (Fig. 3e and Supplementary Fig. S4a), suggesting that both miR-126/miR-126* are protected by Ago proteins, allowing them to regulate their target mRNAs. A similar result was observed in 4T1-C cells (Fig. 3f and Supplementary Fig. S4b), indicating that the expression levels of miR-126/miR-126* do not determine their ability to incorporate into RISC. Using reporter constructs containing the human *Sdf-1α* 3′-UTR with the binding site for either miR-126 ormiR-126* mutated, we found miR-126 and miR-126* RNA mimics to exhibit a strong specificity to their predicted binding site (Fig. 3g). This result is supported by the application of specific locked nucleic acid (LNA) oligonucleotides complementary to either the miR-126 or miR-126* seed sequence[24] to inhibit their functions in cultured cells (Fig. 3h). Together these data suggest that miR-126/miR-126* may act in synergy for maximal effect to suppress Sdf-1α production.

Suppression of MSC recruitment by miR-126/126* through Sdf-1α downregulation

Sdf-1α is known to induce endothelial cell recruitment and promote tumour angiogenesis[25]. Therefore, we reasoned that pri-miR-126 overexpression might inhibit angiogenesis inside the tumour microenvironment by downregulating *Sdf-1α*. However, flow cytometry analysis of dissociated cells from primary tumours revealed that the tumours contained a similar number of $CD31^{+}CD45^{-}$ endothelial cells regardless of pri-miR-126 ectopic expression (Fig. 4a,b). This result was further supported by CD31 immunostaining of those tumours, which showed a similar microvascular density (Fig. 4c,d). The presence of Sdf-1α is also known to correlate with the recruitment of several stem/progenitor cells that express CXCR4, the receptor for Sdf-1α, including haematopoietic stem cells (HSCs), EPCs and MSCs (refs 6,26–29), all of which may contribute to tumour progression and metastasis. However, flow cytometric analysis of primary tumours showed no change in the infiltration of EPCs or HSCs by altered pri-miR-126 expression (Fig. 4e–h).

MSCs were previously reported to promote breast cancer metastasis through the formation of a paracrine loop with tumour cells by educating carcinoma cells to metastasize[7]. To investigate this possibility, we examined whether pri-miR-126 could affect the migratory activity of MSCs *in vitro* using a Transwell assay. Following a previously described procedure[30], MSCs were isolated from the bone marrow of BALB/c mice and seeded into the upper wells of the Transwell chamber. The supernatant from either 4T1-C or 4T1-M cells was added to the lower wells as a chemo-attractant. Consistent with our hypothesis, the number of MSCs that migrated towards the supernatant of 4T1-C cells was significantly greater than that of 4T1-M cells (Fig. 5a). Pre-treatment of MSCs with a CXCR4 antagonist AMD3100, to disrupt the interaction between Sdf-1α and its receptor CXCR4 (ref. 31), significantly impaired their ability to migrate towards the supernatant of 4T1-C cells, suggesting that MSC migration in this system was predominantly regulated by the pri-miR-126/Sdf-1α/CXCR4 axis (Fig. 5a). Consistent with the effect of miR-126/miR-126* on Sdf-1α production, MSC migration was significantly increased when the function of this pair of microRNAs was inhibited by LNA oligonucleotides (Fig. 5b), indicating thatmiR-126/miR-126* may synergize to suppress MSC migration.

Next, we investigated whether endogenous MSC recruitment to the tumour region was affected by changing pri-miR-126 expression *in vivo*. Although it remains unclear whether a set of cell surface markers can specifically identify MSCs without staining other mesenchymal cells inside tumour-associated stroma[32], $Sca\text{-}1^{+}CD44^{+}GFP^{-}CD45^{-}Lin^{-}$ cells are considered to represent mainly MSCs (refs 33,34). We found a significant difference in

the percentage of these cells inside the tumour stroma between 4T1-C- and 4T1-M-initiated tumours (Fig. 5c,d). We next sorted this cell population and cultured them in MSC-specific media, which led to their differentiation into either adipocytes or osteocytes (Fig. 5e), indicating that the tumour-derived Sca-1$^+$CD44$^+$GFP$^-$CD45$^-$Lin$^-$ cells are indeed mesenchymal stem or progenitor cells. We further employed a previously established assay[7] using measurement of colony formation, a hallmark of MSCs, to quantify their frequency within the tumour mass. Specifically, we compared fibroblastoid colony-forming units (CFU-F) generated by tumour-associated stromal cells between the primary tumours formed by GFP-labelled 4T1-C or 4T1-M cells. GFP$^-$ stromal cells isolated from primary tumours in the control group generated more CFU-F than those from tumours with pri-miR-126 overexpression (Fig. 5f). MSCs migrate to primary breast tumours and promote cancer cell migration by releasing the chemokine Ccl5 (ref. 7). Comparison of *Ccl5* mRNA levels in tumours showed that the control group expressed more *Ccl5* (Fig. 5g), consistent with the notion that more MSCs were recruited to 4T1-C-initiated primary tumours. These results strongly suggest that ectopic expression of miR-126/126* suppressed MSC recruitment to the primary tumour site *in vivo*.

miR-126/126* indirectly suppress inflammatory monocyte recruitment *in vivo* by downregulating Ccl2 in an Sdf-1α-dependent manner

Although our results identified *Sdf-1α* as a direct target of miR-126/126*, several other cytokines/chemokines were also found to exhibit differences in their expression profiles (Fig. 2d). Among them was the chemokine *Ccl2*, which was reported to recruit inflammatory monocytes into the tumour microenvironment to facilitate breast cancer metastasis[35]. Analysis of the levels of Gr-1$^+$CD11b$^+$CD115$^+$GFP$^-$ inflammatory monocytes in 4T1-C- and 4T1-M-initiated tumours revealed a significant difference between these two groups (Fig. 6a,b), indicating that Ccl2 might influence the tumour microenvironment by promoting the infiltration of inflammatory monocytes as the second wave of stromal cells recruited following the arrival of MSCs. Interestingly, although inflammatory monocytes are considered as macrophage precursors, no significant difference was observed in the percentage of tumour-associated macrophages between 4T1-C- and 4T1-M-initiated tumours (Supplementary Fig. S5), probably because tumour initiation in the mice for only 10–14 days is too short a time to detect the effect on macrophage accumulation.

In contrast to Sdf-1α, Ccl2 expression is unlikely to be regulated directly by miR-126/126* as our bioinformatics analysis did not identify putative miR-126/miR126* binding sites in the *Ccl2* 3′-UTR. Importantly, *Ccl2* expression was altered only when 4T1 cells grew *in vivo* as primary tumours in the mammary fat pad of BALB/c mice because there was no difference in its mRNA levels in cultured cells (Fig. 6c versus e), in contrast to the expression pattern of *Sdf-1α*. Moreover, in 4T1-M cells, higher mRNA levels of *Sdf-1α* but not *Ccl2* were loaded into the RISC compared with that in 4T1-C cells (Fig. 6d). These results suggest that inside the tumour microenvironment, other cell types, such as the ones recruited by Sdf-1α *in vivo*, may modulate Ccl2 expression in cancer cells. To investigate this possibility, we administrated the CXCR4 antagonist AMD3100 to inhibit the activity of Sdf-1α after inoculating 4T1-C or 4T1-M cancer cells into BALB/c mice. Although *Sdf-1α* was still downregulated in tumours derived from 4T1-M cells, in the AMD3100-treated group *Ccl2* mRNA levels were no longer subject to the inhibitory effect of pri-miR-126 observed in the control group (Fig. 6e), indicating that suppression of Ccl2 production occurs through an Sdf-1α-dependent process, probably through stromal cells, such as MSCs, recruited by Sdf-1α *in vivo*. To explore the clinical relevance of a possible link between *Sdf-1α* and *Ccl2* expression in breast cancer, we analysed the GSE3494 microarray data sets for 251 breast cancer patients and found that the expression levels of these two chemokines are positively correlated (Fig. 6f).

To further investigate the role of Sdf-1α in enhancing the metastatic activities of tumour cells, we conducted further experiments. A derivative of the 4T1 cell line, 66cl4 (ref. 36) was found to express a higher level of miR-126/126* than that of 4T1 cells (Supplementary Fig. S6a). We introduced the sponge constructs that target both miR-126/126* into the 66cl4 cells and found that the level of *Sdf-1α* significantly increased (Supplementary Fig. S6b). When both the 66cl4-sponge-both and 66cl4-control cells were introduced into the mice, a pronounced difference in the survival of those two groups of animals was observed (Supplementary Fig. S6c). In a separate experiment, a 4T1-M-derived cell population (4T1-M-Sdf1) was generated in which pri-miR-126 and *Sdf-1α* complementary DNA without its 3′-UTR, and thus lacking the miR-126/miR-126*-targeting sequences, were co-expressed (Supplementary Fig. S7a,b). The 4T1-M and 4T1-M-Sdf1 cells labelled with luciferase were inoculated and the weight of primary tumours formed by the two types of cell showed no difference (Supplementary Fig. S7c). However, compared with the pri-miR-126-overexpressing group, the 4T1-M-Sdf1 group exhibited much higher luciferase signals for lung metastases 7 or 14 days after surgical removal of primary tumours (Fig. 6g,h), phenocopying the features of the 4T1-C cells shown in Fig. 1f,g. Together, these data indicate that *Sdf-1α* is the most important target for pri-miR-126 to suppress the formation of lung metastases by 4T1 cells.

Epigenetic regulation of miR-126 biogenesis through changes in the methylation status of the host gene *Egfl7* T2 promoter

Clinical data analyses have demonstrated a correlation between reduced expression of miR-126/miR-126* and poor prognosis of breast cancer patients[16], indicating that expression of the miR-126 gene may undergo changes during disease progression. The miR-126 gene is located in an intron of a protein-coding gene, *Egfl7*, and its expression was previously reported to be closely correlated with the T-2 *Egfl7* transcript as illustrated in Fig. 7a (ref. 37). The T-2 promoter contains a large CpG island and miR-126 was previously shown to be upregulated in cancer cell lines treated with inhibitors of DNA methylation and histone deacetylation[37], suggesting that epigenetic regulation of the host *Egfl7* gene could directly affect miR-126/126* expression. Our analyses of miR-126 expression and T-2 *Egfl7* promoter methylation in breast cancer patient tissues showed that samples with highly methylated T-2 promoter exhibited a low expression level of miR-126, whereas samples with a low T-2 promoter methylation level expressed higher levels of miR-126 (Fig. 7b,c). These results indicate that epigenetic changes of the *Egfl7* T-2 promoter are closely correlated with the alterations of miR-126 expression during breast cancer progression.

DISCUSSION

The tumour stromal microenvironment is believed to be critical for the acquisition and maintenance of the metastatic ability of cancer cells, through promoting tumour-associated vasculature formation or by exchanging contextual signals with cancer cells. MicroRNAs have been shown to regulate multiple aspects of the metastatic process, mainly through changes in cancer cell-autonomous characteristics[12]. Our work identified a signalling pathway that regulates the composition of the tumour microenvironment through the action of a pair of microRNAs, miR-126 and miR-126*, which modulate the sequential recruitment of MSCs and inflammatory monocytes into the tumour stroma. The recruited MSCs could form a paracrine loop with the tumour cells to enhance tumour cell invasion and metastasis[7], and possibly the subsequent recruitment of inflammatory monocytes that mainly promote intravasation later in tumour progression[35]. The miR-126/miR-126* target, Sdf-1α, is a multi-functional chemokine secreted by breast cancer cells and cancer-associated stromal cells such as fibroblasts. Sdf-1α can promote tumour cell proliferation and migration through the Sdf-1/CXCR4–Erk signalling pathway[38] and also recruits EPCs, HSCs and

MSCs into the tumour microenvironment from the bone marrow[6,26–29]. The 4T1 murine mammary tumour cells express little CXCR4 (ref. 39) and thus exhibit limited cell-autonomous responses to alterations in Sdf-1α expression (Supplementary Fig. S1). Only the recruitment of MSCs was affected by changes in Sdf-1α production through manipulation of pri-miR-126 in the 4T1-BALB/c model system, probably because of redundant pathways regulating migration of EPCs and HSCs. In contrast to Sdf-1α, Ccl2 expression in cancer cells is indirectly induced by suppressing pri-miR-126, and is probably mediated by other cell types recruited within the tumour mass by Sdf-1α. Ccl2 then recruits inflammatory monocytes as the second wave of stromal cells to further modify the tumour microenvironment. These results suggest that tumour microenvironment alterations could be achieved by a series of events initiated by changes in pri-miR-126 expression. The kinetics of infiltration of different cell types into the tumour stroma and the molecular mechanisms regulating the order of those events will be interesting areas for future experiments.

During the course of this study, miR-126 was reported to suppress lung metastatic colonization by the human breast cancer MDA-MB-231 cells in immune-deficient SCID mice by simultaneously targeting three genes, *IGFBP2, PITPNC1* and *MERTK*, to inhibit endothelial cell recruitment[17]. However, we did not observe any significant differences in lung metastatic nodule number or size when 4T1-C or 4T1-M cells were inoculated intravenously into the BALB/c mice, the same route as that for the MDA-MB-231 cells (Fig. 2a,b). There are several plausible explanations for the different phenotype observed in these two studies. First, we have employed the BALB/c mouse strain for our tumour xenograft model, allowing us to examine the impact of miR-126 on the metastatic capability of tumour cells established in the orthotopic mammary fat pad environment, resembling the primary breast cancer site in humans. This immune-competent host environment provided the biological context to explore the involvement of stromal cells involved in immune regulation and allowed us to observe the sequential recruitment of two different cell types by alterations in miR-126 levels. We have concluded that the predominant impact of miR-126 on breast cancer metastasis in this context is exerted at the primary tumour site, even though we do not rule out that the impact of miR-126 overexpression on lung colonization could be masked by its potent effects in the primary tumour site in our system.

Second, mRNA target selection by miR-126 seems to be context dependent, so that ectopic expression of miR-126 in the two model systems affected different genes to different degrees. As shown in Supplementary Fig. S3, ectopic expression of pri-miR-126 led to significant differences in the expression pattern of four target genes among three cell lines, indicating that their regulation by miR-126/126* is determined by the specific cellular context. It is possible that MDA-MD-231 and 4T1 cells represent different breast cancer cell populations with distinct expression profiles of potential miR-126/126* targets and/or RNA-binding proteins that modulate the accessibility of the putative targets to these microRNAs[40,41]. As a result, pri-miR-126 may suppress the metastatic process through different mechanisms in different subsets of breast cancer patients. Nevertheless, the result of our rescue experiment (Fig. 6g,h) demonstrated that *Sdf-1α* is a key target gene through which miR-126/126* exert their tumour-suppressive effect within the primary tumour microenvironment by inhibiting infiltration of MSCs and inflammatory monocytes. Consequently, this study has provided a distinct mechanism to explain the clinical correlation between reduced expression of miR-126 and poor metastasis-free survival of breast cancer patients.

METHODS

Clinical samples

The tumour specimens and tissue samples used in this study were obtained with informed consent from all subjects in accordance with the Local Ethics Committees of Istituto Scientifico Romagnolo per lo Studio e la Cura dei Tumouri (I.R.S.T.) in Italy and Wenzhou Medical College in China.

Cell culture

The MCF10 cell line series was a gift from L. M. Wakefield at the National Cancer Institute, USA. MCF10 Ca1h and MCF10 Ca1a.c11 cell lines were maintained in DMEM/F-12 supplemented with 5% horse serum and 1% penicillin/streptomycin at 37 °C and 5% CO_2. MCF10 AT1k cells were cultured in a similar medium but additionally with 10 μg ml^{-1} insulin, 20 μg ml^{-1} EGF, 0.5 μg ml^{-1} hydrocortisone and 100 ng ml^{-1} cholera toxin. The 4T1 cells were obtained from ATCC and maintained in RPMI 1640 medium with 10% fetal bovine serum and 1% penicillin/streptomycin. MSCs were isolated from 4- to 6-week-old BALB/c mice according to a published protocol[30] and maintained using the Mouse MesenCult Proliferation Kit (StemCell Technologies).

Reagents and plasmids

AS-miR-126 (5′-TACTCACGGTACG-3′), AS-miR-126* (5′-AAAGTAATAATG-3′) and scramble control LNA oligonucleotides were purchased from Exiqon. Mature miR-126 mimic, miR-126* mimic and control RNA duplexes were obtained from GenePharma. Single-strand miR-126 and miR-126* RNA were purchased from Integrated DNA Technologies. AMD3100 was purchased from Sigma-Aldrich. Pri-miR-126 was inserted into a modified pMSCVpuro Vector (Clontech) together with GFP or the Sdf-1 open reading frame. miR-126 and miR-126* sponge constructs containing ten repeats of anti-sense miR-126 (5′-CGCATTATTAAGTCGGTACGA-3′) or anti-sense miR-126* (5′-CGCGTACCATTCTAATAATG-3′) were designed following the principles previously described[42], synthesized by GenScript and then cloned into the pMSCVpuro Vector (Clontech).

miRNAdetection

The total RNA of cells was isolated with the miRVana extraction kit (Ambion) according to the manufacturer's instructions. We used SYBR-based rtPCR to quantify mature miRNA expression (Quantobio Technology). *Escherichia coli* polyA polymerase was employed to add adenines at the 3′ end of RNA molecules lacking a polyA tail. Following oligo(dT) annealing, a universal tag was attached to the 3′ end of cDNAs during the cDNA synthesis using superscript III reverse transcriptase (Invitrogen). With this universal tag, quantitative PCR was performed with miRNA-specific forward primers and a universal reverse primer mix.

Animal studies

All research involving animals complied with protocols approved by the Duke University Animal Care and Use Committee. For the mammary fat pad metastasis assay, the indicated numbers of luciferase-labelled 4T1-C, 4T1-M or 4T1-SP-both tumour cells were inoculated into the mammary fat pad of 6–8-week-old female BALB/c mice following an established protocol[19]. After 10 days, the tumours were surgically removed and weighed. Metastatic lung lesion formation was monitored by the appearance of luciferase activity using imaging apparatus (IVIS systems). For the tail vein metastasis assay, 5×10^5 4T1-C or 4T1-M cells were inoculated intravenously into 6–8-week-old female BALB/c mice as previously

described[43], and the lungs were removed two weeks later and fixed with Bouin's solution. For the AMD3100 treatment, GFP-labelled 4T1-C or 4T1-M cells were inoculated into the mammary fat pad as previously described. AMD3100 (150 μg) was given subcutaneously to the area surrounding the fat pad every other day, a slight modification of a published procedure[44], beginning after cancer cell inoculation and continuing until the tumours were removed.

Luciferase reporter assay

The human SDF-1A 3′-UTR or the mouse Sdf-1α 3′-UTR containing the predicted binding sites for both miR-126 and miR- 126* was cloned into the pmiR-GLO dual luciferase reporter plasmid (Promega) downstream of the firefly luciferase coding region. Corresponding reporters containing mutations in the seed regions of both miR-126 and miR-126* binding sites were generated using the QuikChange II Site-Directed Mutagenesis Kit (Agilent Technologies) following the manufacturer's instructions. The pri-miR-126Mut construct was generated through synthesizing DNA sequences containing described mutations (Integrated DNA Technologies), annealing and then cloning into the pMSCVpuro vector (Clontech). HEK293T cells were co-transfected with the pmiR-GLO reporter and MSCV–control, MSCV–Pri-miR-126 or MSCV–Pri-miR-126 Mut plasmids. Cells were lysed 48 h after transfection and analysed for firefly and *Renilla* luciferase activities using the Dual-Luciferase Assays (Promega) on a VICTOR3 multilabel reader (PerkinElmer).

Western blots

For protein quantification, total cell extracts or concentrated supernatants were fractionated by electrophoresis on a gradient SDS polyacrylamide gel (Invitrogen) and transferred onto a PVDF membrane. The final results were quantified using ImageJ software. Western blotting was performed with the following primary antibodies: anti-Sdf1α from Abcam (catalogue number ab25117, polyclonal, 1:1,000 dilution), anti--tubulin from Santa Cruz (catalogue number sc-7396, polyclonal, 1:2,000 dilution), anti-pan Ago from Millipore (catalogue number MABE56, monoclonal 2A8, 1:1,000 dilution) and anti-β-actin from Sigma (catalogue number A5441, monoclonal AC-15, 1:5,000 dilution).

RNA immunoprecipitation

Following a previously published procedure[45,46], 80% confluent 4T1-M cells were washed with ice-cold PBS and irradiated in a Stratalinker, and then cells were collected and lysed in 1× PXL buffer (1 × PBS. 0.1%SDS, 0.5% deoxycholate and 0.5% NP-40) with a complete EDTA-free proteinase inhibitor (Roche) and an RNase Inhibitor (Applied Biosystems) for 10 min on ice. Beads with bound antibody were prepared using protein-A DynaBeads (Invitrogen). The beads were first incubated with a bridging rabbit anti-mouse antibody (Jackson ImmunoResearch Laboratories) for 45 min at room temperature, then washed with phosphate buffer and incubated with 10 μl of anti-pan Ago clone 2A8 (Millipore) or mouse IgG (Jackson ImmunoResearch Laboratories) for 4 h at 4 °C. After 3 washes with 1× PXL buffer, the beads were incubated with cell lysates for 2 h at 4 °C. They were subsequently washed 3 times using 3× PXL buffer. Affiliated RNA was released by proteinase K treatment for 40 min at 37 °C and then precipitated with ethanol. The RNA was either used for miRNA detection as previously described or for mRNA analysis following reverse transcription with random primers (Invitrogen).

Real-time PCR analysis

To detect mRNA expression levels, total RNA was isolated with Trizol (Sigma) according to the manufacturer's instructions. Total RNA or Ago-affiliated RNA was then processed for rtPCR analysis for different genes using the following forward and reverse primers:

mSdf-1α-left, 5′-CTGTGCCCTTCAGATTGTTG-3′, mSdf-1α-right, 5′-TCAGCCTTCCTCGGGGGTCT-3′; mCcl2-left, 5′-AAAATCATCCAAAAGATACTGAACAA-3′, mCcl2-right, 5′-CTTTGGTTCTTCCGTTGAGG-3′; mIGFBP2-left, 5′-GCGGGTACCTGTGAAAAGAG-3′, mIGFBP2-right, 5′-CCTCAGAGTGGTCGTCATCA-3′; mPITPNC1-left, 5′-ACCAACATAAAAGTTTGCAATCAG-3′, mPITPNC1-right, 5′-CGCACTTCATCCATTGTCAT-3′; mMERTK-left, 5′-GAGGACTGCTTGGATGAACTGTA-3′, mMERTK-right, 5′-AGGTGGGTCGATCCAAGG-3′.

MSC migration assays

MSCs with or without AMD3100 treatment were layered in the upper well of a 24-well Transwell chamber (Corning) and allowed to migrate towards cell-free media placed in the bottom wells, derived from 4T1-C or 4T1-M cells. Membranes were processed following standard protocols. Migrating cells were stained using 0.5% toluidine blue in 4% PFA and counted using bright-field microscopy.

Flow cytometry and CFU-F studies

Tumour xenografts were implanted in 6–8-week-old BALB/c female mice and allowed to grow as indicated. For flow cytometry, tumours were excised, treated with collagenase, and cells were then strained and stained with fluorescence-conjugated antibodies and analysed on a FACS Canto machine (Becton-Dickinson) according to the manufacturer's instructions. Antibodies included PE anti-mouse CD31 (PECAM-1; catalogue number 12-0311-81, clone 390, at 5 ng μl^{-1}), PerCP-Cy5.5 anti-mouse CD45.2 (catalogue number 45-0454-82, clone 104, at 10 ng μl^{-1}), PE anti-mouse CD117 (c-Kit; catalogue number 12-1171-82, clone 2B8, at 1.25 ng μl^{-1}), APC anti-mouse Ly-6A/E (Sca-1; catalogue number 17-5981-81, clone D7, at 0.6 ng μl^{-1}), PE anti-human/mouse CD44 (catalogue number 12-0441-81, clone IM7, at 1.25 ng μl^{-1}), eFluor450 mouse haematopoietic lineage cocktail (including eFluor450 anti-mouse CD3, CD45R, CD11b, TER-119 and Gr-1; catalogue number 88-7772-72, clone 17A2, RA3-6B2, M1/70, TER-119, RB6-8C5, dilution 1.5), eFluor450 anti-mouse Ly-6G (Gr-1; catalogue number 48-5931-80, clone RB6-8C5, at 0.6 ng μl^{-1}), PE anti-mouse CD115 (catalogue number 12-1152-81, clone AFS98, at 0.6 ng μl^{-1}), PerCP-Cy5.5 anti-mouse CD11b (catalogue number 45-0112-80, clone M1/70, at 2.5 ng μl^{-1}) and APC anti-mouse F4/80 (catalogue number 17-4801-80, clone BM8, at 20 ng μl^{-1}) obtained from eBioscience. For CFU-F detection, tumours were excised, treated with collagenase, and the GFP^- tumour stromal cells were isolated from the GFP^+ cancer cells using FACS. CFU-F culture assays were performed on the sorted mouse stromal population as described previously[7]. Colonies were stained 14 days later using the Giemsa stain and quantified under light microscopy.

Tumour-derived MSC differentiation assay

$Sca\text{-}1^+CD44^+CD45^-Lin^-GFP^-$ cells were isolated from 4T1-C-initiated tumours and cultured in MSC-specific medium (StemCell Technologies). Five days later, these cells were seeded into 24-well plates at a density of 1×10^4 per well, and then induced to differentiate into either adipocytes or osteocytes using the Mouse MSC Functional Identification Kit from R&D systems following the manufacturer's instruction. The medium was changed twice a week for another 20 days. Adipocytes were visualized using red oil staining; osteocytes were identified by using an antibody against osteopontin.

Bisulphite modification and genomic sequencing

The methylation status of the CpG dinucleotides close to the *Egfl7* T-2 promoter was analysed. A bisulphite sequencing assay was performed on 1.0 mg of bisulphite-treated genomic DNA from the clinical samples. Bisulphite conversion was performed using the MethylDetector Bisulfite Modification Kit (Active Motif) according to the manufacturer's instructions. The fragments of interest were amplified using the following specific primer pairs designed with the MethPrimer software[47]: forward, 5′-TTGGGTTTTGTTATGTGGTTTTAG-3′; reverse, 5′-AACCCTTTACTAACTTTCAAACCC-3′. PCR products were gel purified and cloned into the pCR4-TOPO TA vectors (Invitrogen). Individual bacterial colonies were picked and sequenced using the M13 Reverse primer (5′-GTTTTCCCAGTCACGAC-3′) to analyse DNA methylation.

Statistical methods

For statistical analyses, mean values with standard deviation (s.d.) are shown in most graphs that were generated from several repeats of biological experiments. *P* values were obtained from *t*-tests with paired or unpaired samples, with significance set at $P < 0.05$.

Microarray data access

The miRNA profiling of MCF10-derived cell series and cytokine/chemokine array results of tumour-derived 4T1-C and 4T1-M cells have been deposited in the NCBI Gene Expression Omnibus and are accessible through GEO series accession numbers GSE42884 and GSE42885 http://www.ncbi.nlm.nih.gov/geo/query/acc.cgi?acc=GSE42884, http://www.ncbi.nlm.nih.gov/geo/query/acc.cgi?acc=GSE42885.

The clinical data set used to analyse the relationship between CXCL12 and CCL2 expression is accessible through GEO series accession number GSE3494 http://www.ncbi.nlm.nih.gov/geo/query/acc.cgi?acc=GSE3494.

Supplementary Material

Refer to Web version on PubMed Central for supplementary material.

Acknowledgments

The authors thank R. A. Weinberg, L. M. Wakefield, C. Counter and A. M. Pendergast for providing reagents. We also thank G. J. Markowitz for thoughtful comments on the manuscript. This work was supported by the NIH grant CA151541 to X-F.W., the S. G. Komen For The Cure Foundation grant KG101633 to X-F.W. (PI) and X.X. (Fellow), the Research Scholar Grant RSG-10-157-01-LIB from the American Cancer Society to Q-J.L. and Ministry of Science and Technology Key Program of China 2012ZX10002009-017, National Basic Research Program of China 2010CB912102 to D.X.

References

1. Parkin DM, Bray F, Ferlay J, Pisani P. Global cancer statistics, 2002. CA Cancer J. Clin. 2005; 55:74–108. [PubMed: 15761078]
2. Nguyen DX, Bos PD, Massague J. Metastasis: from dissemination to organ-specific colonization. Nat. Rev. Cancer. 2009; 9:274–284. [PubMed: 19308067]
3. Valastyan S, Weinberg RA. Tumour metastasis: molecular insights and evolving paradigms. Cell. 2011; 147:275–292. [PubMed: 22000009]
4. Chaffer CL, Weinberg RA. A perspective on cancer cell metastasis. Science. 2011; 331:1559–1564. [PubMed: 21436443]

5. Hanahan D, Coussens LM. Accessories to the crime: functions of cells recruited to the tumour microenvironment. Cancer Cell. 2012; 21:309–322. [PubMed: 22439926]
6. Orimo A, et al. Stromal fibroblasts present in invasive human breast carcinomas promote tumour growth and angiogenesis through elevated SDF-1/CXCL12 secretion. Cell. 2005; 121:335–348. [PubMed: 15882617]
7. Karnoub AE, et al. Mesenchymal stem cells within tumour stroma promote breast cancer metastasis. Nature. 2007; 449:557–563. [PubMed: 17914389]
8. Li HJ, Reinhardt F, Herschman HR, Weinberg RA. Cancer-stimulated mesenchymal stem cells create a carcinoma stem cell niche via prostaglandin E2 signaling. Cancer Discov. 2012; 2:840–855. [PubMed: 22763855]
9. Hanahan D, Weinberg RA. Hallmarks of cancer: the next generation. Cell. 2011; 144:646–674. [PubMed: 21376230]
10. Joyce JA, Pollard JW. Microenvironmental regulation of metastasis. Nat. Rev. Cancer. 2009; 9:239–252. [PubMed: 19279573]
11. Bartel DP. MicroRNAs: genomics, biogenesis, mechanism, and function. Cell. 2004; 116:281–297. [PubMed: 14744438]
12. Nicoloso MS, Spizzo R, Shimizu M, Rossi S, Calin GA. MicroRNAs–the micro steering wheel of tumour metastases. Nat. Rev. Cancer. 2009; 9:293–302. [PubMed: 19262572]
13. Kasinski AL, Slack FJ. Epigenetics and genetics. MicroRNAs en route to the clinic: progress in validating and targeting microRNAs for cancer therapy. Nat. Rev. Cancer. 2011; 11:849–864. [PubMed: 22113163]
14. Volinia S, et al. A microRNA expression signature of human solid tumours defines cancer gene targets. Proc. Natl Acad. Sci. USA. 2006; 103:2257–2261. [PubMed: 16461460]
15. Ma L, Teruya-Feldstein J, Weinberg RA. Tumour invasion and metastasis initiated by microRNA-10b in breast cancer. Nature. 2007; 449:682–688. [PubMed: 17898713]
16. Tavazoie SF, et al. Endogenous human microRNAs that suppress breast cancer metastasis. Nature. 2008; 451:147–U143. [PubMed: 18185580]
17. Png KJ, Halberg N, Yoshida M, Tavazoie SF. A microRNA regulon that mediates endothelial recruitment and metastasis by cancer cells. Nature. 2012; 481:190–194. [PubMed: 22170610]
18. Crawford M, et al. MicroRNA-126 inhibits invasion in non-small cell lung carcinoma cell lines. Biochem. Biophys. Res. Commun. 2008; 373:607–612. [PubMed: 18602365]
19. Dong M, et al. The type III TGF-beta receptor suppresses breast cancer progression. J. Clin. Invest. 2007; 117:206–217. [PubMed: 17160136]
20. Yang P, et al. TGF-beta-miR-34a-CCL22 signaling-induced treg cell recruitment promotes venous metastases of HBV-positive hepatocellular carcinoma. Cancer Cell. 2012; 22:291–303. [PubMed: 22975373]
21. Miranda KC, et al. A pattern-based method for the identification of microRNA binding sites and their corresponding heteroduplexes. Cell. 2006; 126:1203–1217. [PubMed: 16990141]
22. Betel D, Wilson M, Gabow A, Marks DS, Sander C. The microRNA.org resource: targets and expression. Nucl. Acids Res. 2008; 36:D149–D153. [PubMed: 18158296]
23. Kim VN, Han J, Siomi MC. Biogenesis of small RNAs in animals. Nat. Rev. Mol. Cell Biol. 2009; 10:126–139. [PubMed: 19165215]
24. Stenvang J, Petri A, Lindow M, Obad S, Kauppinen S. Inhibition of microRNA function by antimiR oligonucleotides. Silence. 2012; 3:1. [PubMed: 22230293]
25. Kryczek I, et al. CXCL12 and vascular endothelial growth factor synergistically in- duce neoangiogenesis in human ovarian cancers. Cancer Res. 2005; 65:465–472. [PubMed: 15695388]
26. Aiuti A, Webb IJ, Bleul C, Springer T, GutierrezRamos JC. The chemokine SDF-1 is a chemoattractant for human CD34(+) hematopoietic progenitor cells and provides a new mechanism to explain the mobilization of CD34(+) progenitors to peripheral blood. J. Exp. Med. 1997; 185:111–120. [PubMed: 8996247]
27. Ponte AL, et al. The *in vitro* migration capacity of human bone marrow mesenchymal stem cells: comparison of chemokine and growth factor chemotactic activities. Stem Cells. 2007; 25:1737–1745. [PubMed: 17395768]

28. Kitaori T, et al. Stromal cell-derived factor 1/CXCR4 signalling is critical for the recruitment of mesenchymal stem cells to the fracture site during skeletal repair in a mouse model. Arthritis Rheum. 2009; 60:813–823. [PubMed: 19248097]
29. Son BR, et al. Migration of bone marrow and cord blood mesenchymal stem cells in vitro is regulated by stromal-derived factor-1-CXCR4 and hepatocyte growth factor-c-met axes and involves matrix metalloproteinases. Stem Cells. 2006; 24:1254–1264. [PubMed: 16410389]
30. Soleimani M, Nadri S. A protocol for isolation and culture of mesenchymal stem cells from mouse bone marrow. Nat. Protoc. 2009; 4:102–106. [PubMed: 19131962]
31. Broxmeyer HE, et al. Rapid mobilization of murine and human hematopoietic stem and progenitor cells with AMD3100, a CXCR4 antagonist. J. Exp. Med. 2005; 201:1307–1318. [PubMed: 15837815]
32. Fox JM, Chamberlain G, Ashton BA, Middleton J. Recent advances into the understanding of mesenchymal stem cell trafficking. Br. J. Haematol. 2007; 137:491–502. [PubMed: 17539772]
33. Meirelles Lda S, Nardi NB. Murine marrow-derived mesenchymal stem cell: isolation, in vitro expansion, and characterization. Br. J. Haematol. 2003; 123:702–711. [PubMed: 14616976]
34. Baddoo M, et al. Characterization of mesenchymal stem cells isolated from murine bone marrow by negative selection. J. Cell Biochem. 2003; 89:1235–1249. [PubMed: 12898521]
35. Qian BZ, et al. CCL2 recruits inflammatory monocytes to facilitate breast-tumour metastasis. Nature. 2011; 475:222–225. [PubMed: 21654748]
36. Aslakson CJ, Miller FR. Selective events in the metastatic process defined by analysis of the sequential dissemination of subpopulations of a mouse mammary tumour. Cancer Res. 1992; 52:1399–1405. [PubMed: 1540948]
37. Saito Y, et al. Epigenetic therapy upregulates the tumour suppressor microRNA-126 and its host gene EGFL7 in human cancer cells. Biochem. Biophys. Res. Commun. 2009; 379:726–731. [PubMed: 19116145]
38. Marchesi F, et al. Increased survival, proliferation, and migration in metastatic human pancreatic tumour cells expressing functional CXCR4. Cancer Res. 2004; 64:8420–8427. [PubMed: 15548713]
39. Miao Z, et al. CXCR7 (RDC1) promotes breast and lung tumour growth *in vivo* and is expressed on tumour-associated vasculature. Proc. Natl Acad. Sci. USA. 2007; 104:15735–15740. [PubMed: 17898181]
40. Kedde M, et al. RNA-binding protein Dnd1 inhibits microRNA access to target mRNA. Cell. 2007; 131:1273–1286. [PubMed: 18155131]
41. Kedde M, et al. A Pumilio-induced RNA structure switch in p27-3′ UTR controls miR-221 and miR-222 accessibility. Nat. Cell Biol. 2010; 12:1014–1020. [PubMed: 20818387]
42. Ebert MS, Neilson JR, Sharp PA. MicroRNA sponges: competitive inhibitors of small RNAs in mammalian cells. Nat. Methods. 2007; 4:721–726. [PubMed: 17694064]
43. Ma C, et al. Extracellular matrix protein betaig-h3/TGFBI promotes metastasis of colon cancer by enhancing cell extravasation. Genes Dev. 2008; 22:308–321. [PubMed: 18245446]
44. Rubin JB, et al. A small-molecule antagonist of CXCR4 inhibits intracranial growth of primary brain tumours. Proc. Natl Acad. Sci. USA. 2003; 100:13513–13518. [PubMed: 14595012]
45. Chi SW, Zang JB, Mele A, Darnell RB. Argonaute HITS-CLIP decodes microRNA-mRNA interaction maps. Nature. 2009; 460:479–486. [PubMed: 19536157]
46. Ule J, et al. CLIP identifies Nova-regulated RNA networks in the brain. Science. 2003; 302:1212–1215. [PubMed: 14615540]
47. Li LC, Dahiya R. MethPrimer: designing primers for methylation PCRs. Bioinformatics. 2002; 18:1427–1431. [PubMed: 12424112]

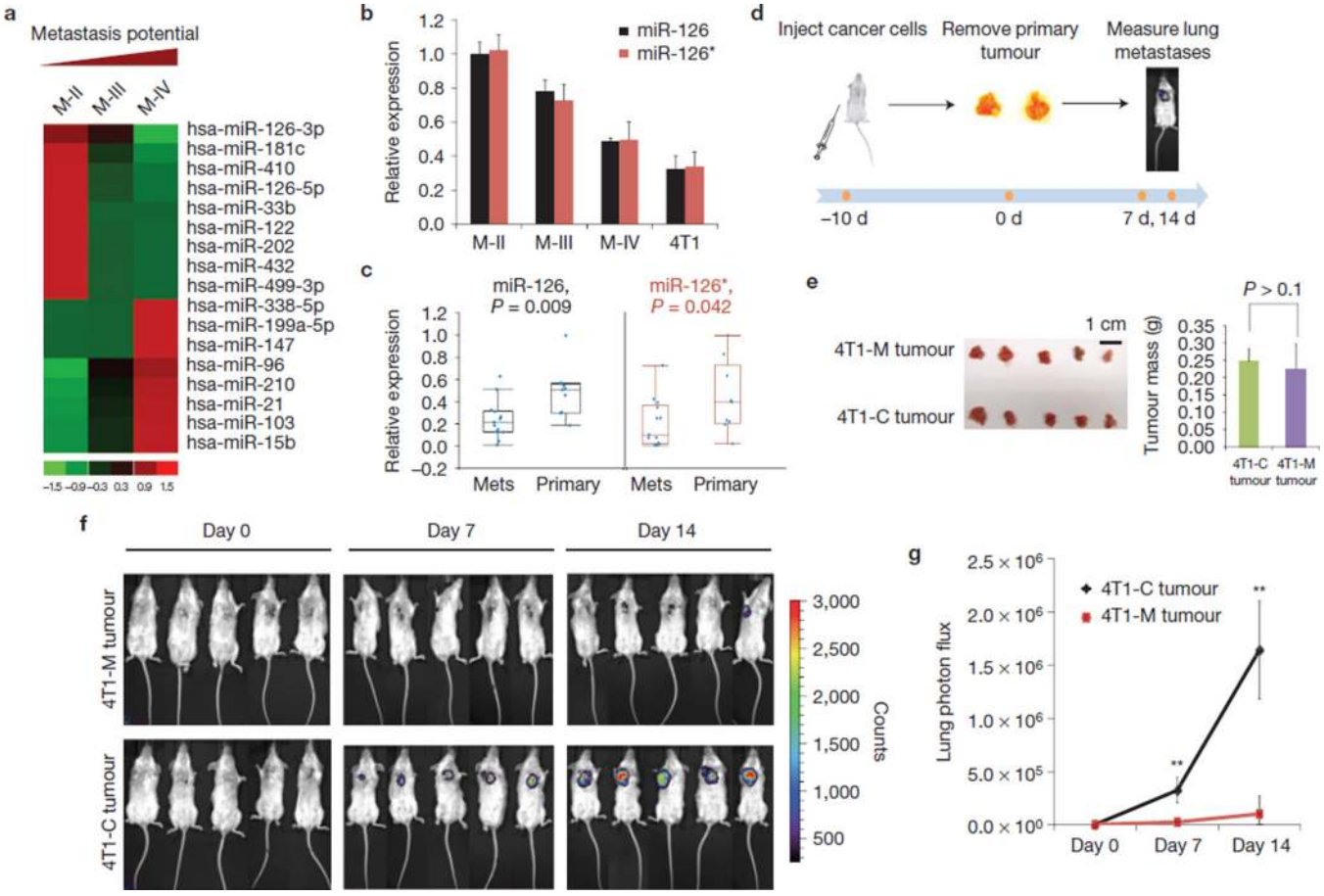

Figure 1.

Identification of miR-126 and miR-126* as potential suppressors of breast cancer metastasis. (**a**) A partial list of microRNAs whose expression pattern correlates with metastatic potential in M-II (MCF10 AT1k, benign), M-III (MCF10 Ca1h, low metastatic) and M-IV (MCF10 Ca1a.c11, high metastatic) cells. A total of 242 microRNAs were tested in a quantitative-rtPCR-based array as previously described[20]. Data were normalized using U6 RNA. (**b**) miR-126 and miR-126* expression were inversely correlated with metastatic potential. The relative expression levels of miR-126 and miR-126* were measured by quantitative rtPCR and normalized to U6 RNA. The data presented are shown as mean±s.d. collected from three independent experiments. (**c**) miR-126 and miR-126* are expressed at a higher level in primary breast tumours than in metastatic tumour samples. The relative expression levels of miR-126 and miR-126* in 9 primary and 13 metastatic tissues were measured by quantitative rtPCR and normalized to U6 RNA. In the box-and-whisker plot, each point represents one sample. The central box represents the values from the lower to upper quartile. The middle line represents the median. The horizontal line extends from the minimum to the maximum value excluding far-out values. (**d**) Schematic procedure of *in vivo* tumour implantation and lung metastases measurement. (**e**) Pri-miR-126 ectopic expression had little impact on primary tumour size or weight. Approximately 5×10^4 control or ectopic pri-miR-126-expressing 4T1 cells harbouring a luciferase reporter were implanted into the mammary fat pad of 6-week-old female BALB/c mice. After 10 days, tumours grown at the primary site were surgically removed and weighed. The data presented are shown as mean±s.d. collected from five independent experiments. (**f**) Pri-miR-126 suppressed the formation of lung metastases by 4T1 cells. Metastatic lung lesion formation

was monitored by the appearance of luciferase activity using imaging apparatus 7 and 14 days after primary tumour removal, $n = 5$ in each group. (**g**) Quantification of the results shown in **f**. The data are shown as mean±s.d. collected from five independent experiments. $^{**}P < 0.01$.

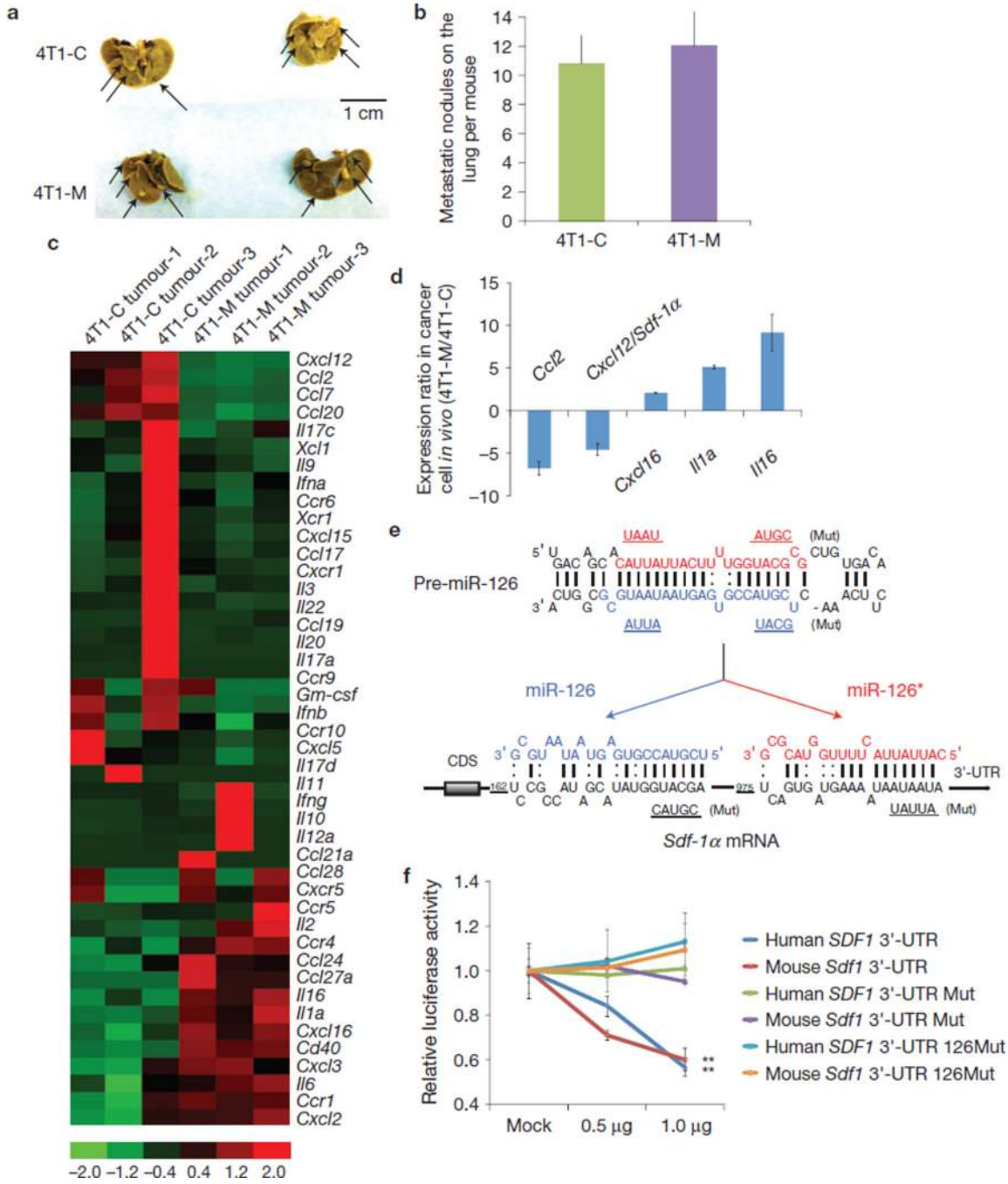

Figure 2.

Identification of *Sdf-1α* as a target for miR-126/126*. (**a**) Representative lung images showing the metastatic nodules formed two weeks after 4T1-C and 4T1-M cells were intravenously inoculated into BALB/c mice through the tail vein. The lung tissues were stained with Bouin's solution. Arrows indicate metastatic nodules. (**b**) Quantification of he number of metastatic nodules on the lungs formed by 4T1-C and 4T1-M cells. The data presented are shown as mean±s.d. collected from five independent experiments. (**c**) List of cytokines and chemokines or their receptors with a more than twofold expression difference between carcinoma cells dissociated from 4T1-C and 4T1-M cell-derived tumours *in vivo*.

Tumour samples from three mice for each cell type were used in the analysis as indicated. (**d**) Five cytokines and chemokines with significantly altered expression ($P < 0.05$) from the list in **c** were confirmed using quantitative rtPCR and normalized with β-actin. The data presented are shown as mean±s.d. collected from three independent experiments. (**e**) The 3′-UTR of the *Sdf-1α* gene contains binding sites for both miR-126 and miR-126* according to bioinformatic analysis. Coloured underlined sequences show the point mutations used to generate the pri-miR-126Mut construct. Black underlined sequences show the point mutations used to generate human and mouse *Sdf-1α* 3′-UTR Mut constructs. (**f**) Pri-miR-126 suppressed the expression of a luciferase reporter gene harbouring the 3′-UTR of *Sdf-1α*. The pmiRGLO plasmid was modified by adding the human or mouse wild-type *Sdf-1α* 3′-UTR or the 3′-UTRs with mutations in regions complementary to both the miR-126 and miR-126* seed regions behind the firefly luciferase gene. HEK293T cells were transiently co-transfected with negative control (mock) or pri-miR-126 together with the indicated luciferase constructs, and luciferase activity was analysed 48 h later. Data are presented as relative firefly luciferase activity normalized to *Renilla* luciferase activity from the same construct. The data presented are shown as mean±s.d. collected from three independent experiments. $^{**}P < 0.01$.

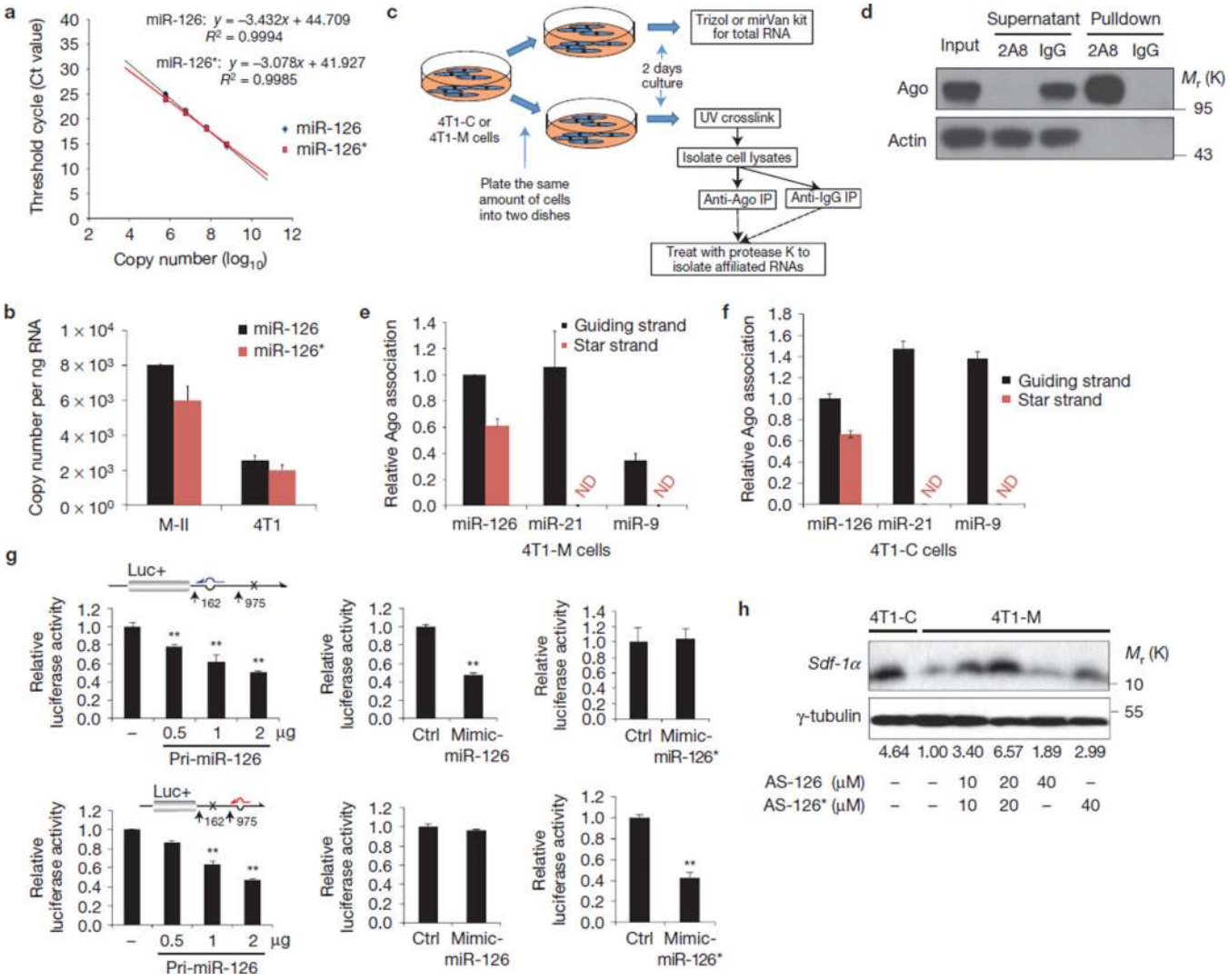

Figure 3.

miR-126 and miR-126* regulate *Sdf-1α* independently. (**a**) Correlation of RNA input to the threshold of cycle (Ct) values for miR-126 and miR-126*. Single-strand miR-126 or miR-126* RNA input ranged from 10^{-10} to 10^{-3} pmol per RT reaction. (**b**) Quantitative rtPCR demonstrated similar miR-126 and miR-126* expression in M-II or 4T1 cells. The data presented are shown as mean±s.d. collected from three independent experiments. The standard curve generated in **a** was used to calculate the copy numbers. (**c**) The procedure for anti-Ago RNA immunoprecipitation (IP). Cells (4T1-C or 4T1-M) were divided into two parts for total RNA extraction (upper arrow) and anti-Ago immunoprecipitation followed by RNA extraction (lower arrow). (**d**) Western blot shows the specificity and efficiency of anti-Ago immunoprecipitation using 4T1-M cells; 2A8 is an anti-Ago antibody. (**e**) Both miR-126 and miR-126* incorporate into RISC in 4T1-M cells. RISC-associated microRNAs were examined by quantitative rtPCR in the immunoprecipitates generated using an anti-Ago antibody from 4T1-M cells, and normalized by comparison with their expression levels in whole-cell lysates. The data presented are shown as mean±s.d. collected from three independent experiments. ND, undetectable. (**f**) Both miR-126 and miR-126* incorporate into RISC in 4T1-C cells. The data presented are shown as mean±s.d. collected from 3 independent experiments. (**g**) miR-126 and miR-126* regulate SDF-1A expression

independently. The pmiRGLO plasmid containing the 3′-UTR of mouse SDF-1A was modified into two plasmids containing the intact binding site for either miR-126 or miR-126* alone (blue represents miR-126; red represents miR-126*). These two plasmids were co-transfected with pri-miR-126, mimic miR-126 RNA duplex or mimic miR-126* RNA duplex separately. The data presented are shown as mean±s.d. collected from three independent experiments. (**h**) Western blotting was used to analyse the presence of Sdf-1α in the concentrated supernatant from 4T1-C or 4T1-M cells treated with anti-miR-126 or anti-miR-126* LNA oligonucleotides at the indicated concentrations. The whole-cell lysate from each sample of cells from which the supernatant was collected was blotted with anti-tubulin antibody as a loading control. The results were quantifed using ImageJ and normalized results are shown under the blots. Uncropped images of blots are shown in Supplementary Fig. S8.

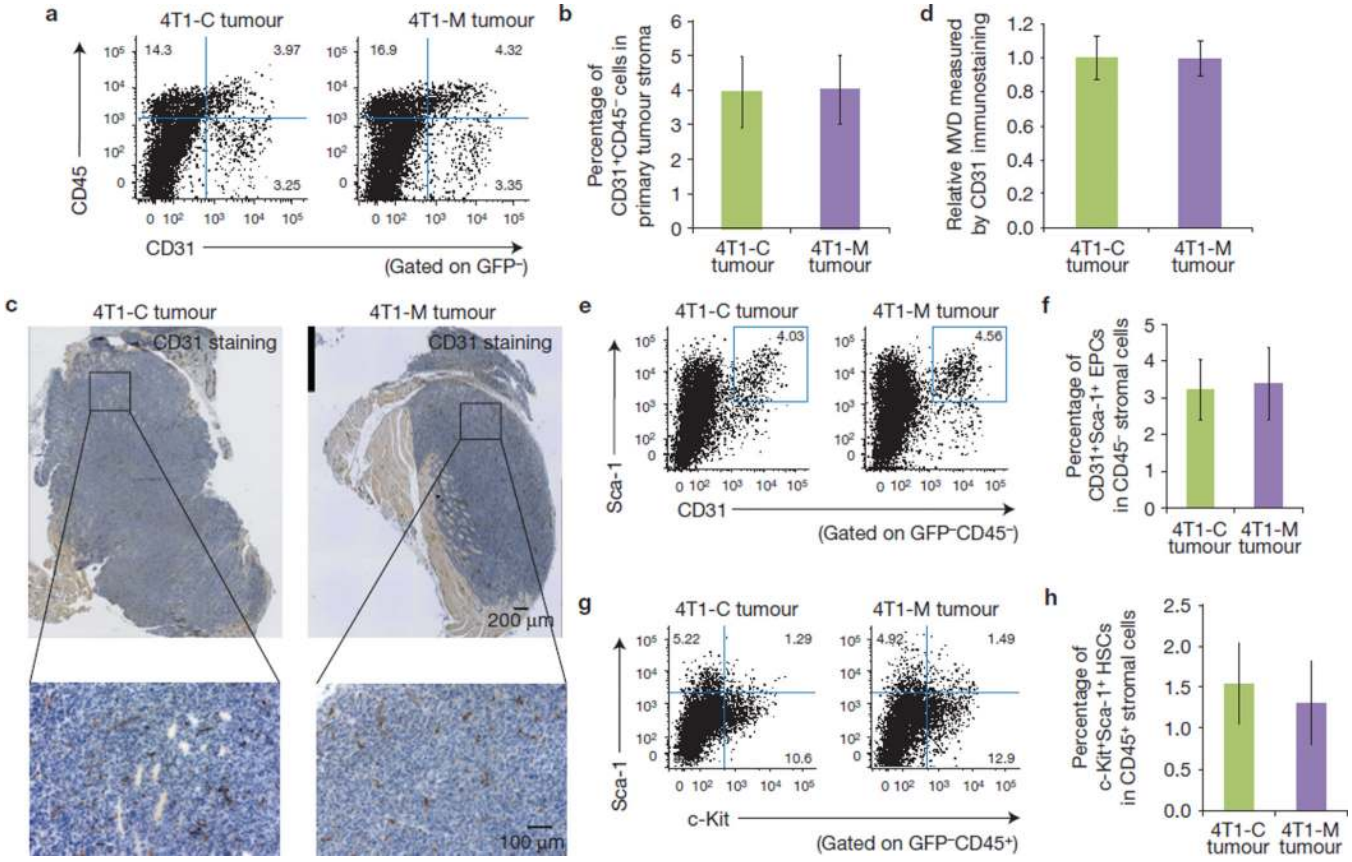

Figure 4.

miR-126/miR-126* do not suppress tumour angiogenesis or the recruitment of HSCs and EPCs. (**a**) Fluorescence-activated cell sorting (FACS) analysis of tumours showing the proportion of $CD45^{-}CD31^{+}$ endothelial cells inside the GFP^{-} tumour-associated stroma. (**b**) Quantification of the percentage of endothelial cells in 4T1-C and 4T1-M tumour stroma. Error bars represent mean±s.d. collected from three independent experiments. $P > 0.1$ by Student's *t*-test, indicating no statistical significance. (**c**) Representative CD31 immunostaining of 4T1-C- and 4T1-M-initiated tumours. Scale bars, 200 μm (upper panels) and 100 μm (lower panels). (**d**) Relative microvascular density (MVD) determined by CD31 staining. Five random fields in each tumour were counted for MVD. Error bars represent mean±s.d. from three independent experiments. $P > 0.1$ by Student's *t*-test, indicating no statistical significance. (**e**) FACS analysis of tumours showing the proportion of $CD31^{+}Sca\text{-}1^{+}$ EPCs inside the GFP^{-} tumour-associated stroma. (**f**) Quantification of the percentage of EPCs in 4T1-C and 4T1-M tumour stroma. Error bars represent mean±s.d. collected from three independent experiments. $P > 0.1$ by Student's *t*-test, indicating no statistical significance. (**g**) FACS analysis of tumours showing the proportion of $CD45^{+}Sca\text{-}1^{+}c\text{-}Kit^{+}$ HSCs inside the GFP^{-} tumour-associated stroma. (**h**) Quantification of the percentage of HSCs in 4T1-C and 4T1-M tumours. Error bars represent mean±s.d. collected from three independent experiments. $P > 0.1$ by Student's *t*-test, indicating no statistical significance.

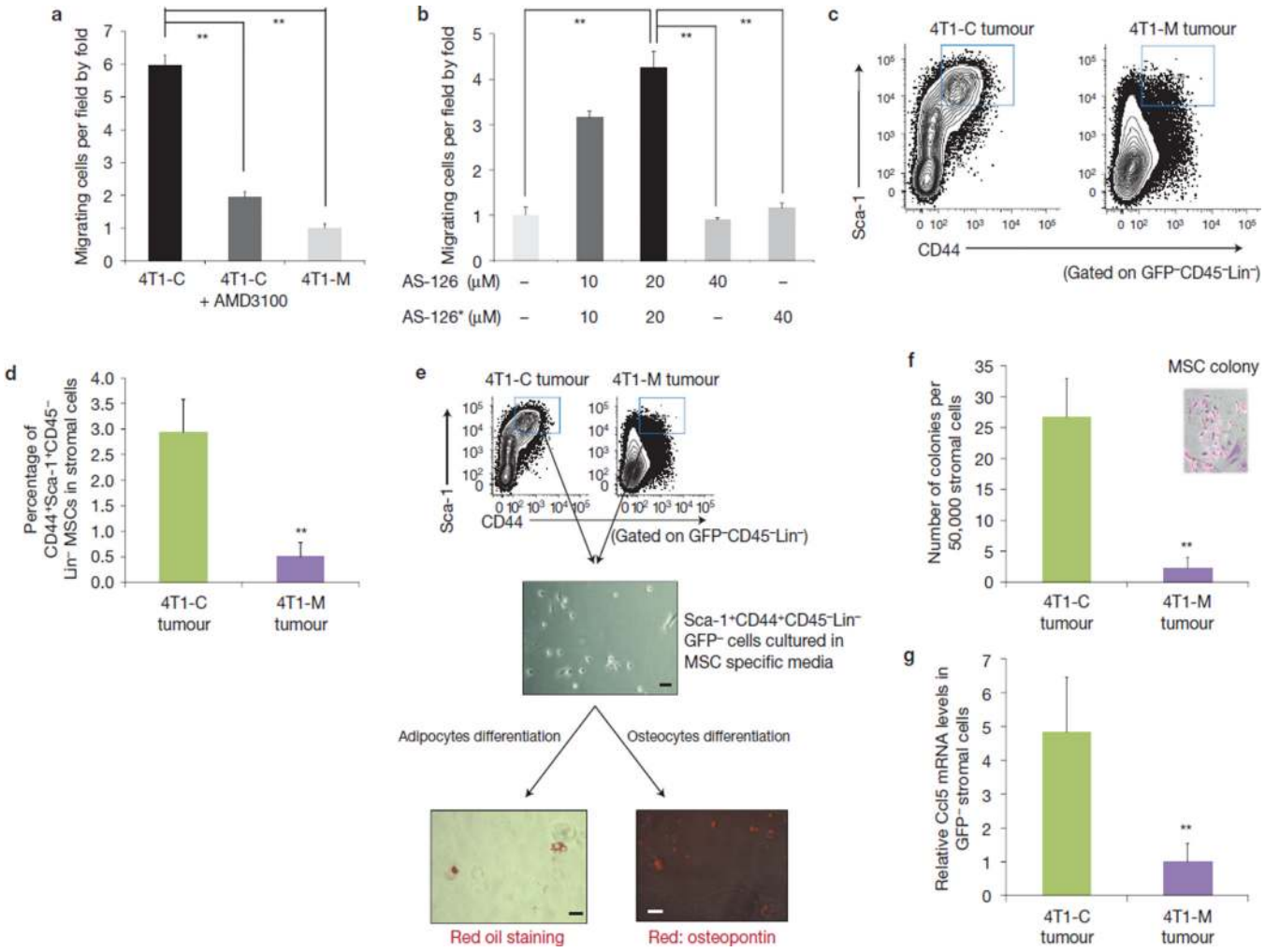

Figure 5.

miR-126/miR-126* suppress MSC migration through downregulating Sdf-1α *in vitro* and *in vivo*. (**a**) Migrating capability of MSCs towards supernatants from 4T1-C or 4T1-M cells. Approximately 5×10^4 mouse MSCs were used for each Transwell assay over a period of 18 h. For AMD3100 treatment, MSCs were cultured in the presence of AMD3100 at the indicated concentration for 24 h before being plated into the upper chamber. Data are presented as mean±s.d. from three independent experiments. In each experiment, five random fields were counted to measure the migrating MSCs. (**b**) Results of a similar experiment as in **a** except that the cancer cells were treated with anti-miR-126 or anti-miR-126* LNA oligonucleotides for 24 h before the supernatant was collected. The concentrations of LNA oligonucleotides are indicated. Data are presented as mean±s.d. from three independent experiments. In each experiment, five random fields were counted to measure the migrating MSCs. (**c**) FACS analysis of tumours showing the proportion of Sca-1$^+$CD44$^+$CD45$^-$Lin$^-$GFP$^-$ MSCs inside the tumour-associated GFP$^-$ stroma. (**d**) Quantification of the percentage of Sca-1$^+$CD44$^+$CD45$^-$Lin$^-$GFP$^-$ MSCs in 4T1-C- and 4T1-M-initiated tumour stroma. The data presented are shown as mean±s.d. collected from three independent experiments. (**e**) The tumour-derived Sca-1$^+$CD44$^+$CD45$^-$Lin$^-$GFP$^-$ population is able to differentiate into adipocytes and osteocytes. Sca-1$^+$CD44$^+$CD45$^-$Lin$^-$GFP$^-$ cells were isolated and cultured in MSC-specific medium (StemCell Technologies). These cells were then induced to differentiate into either

adipocytes or osteocytes using the Mouse MSC Functional Identification Kit from R&D systems. Adipocytes were visualized using red oil staining. Osteocytes were identified by using an antibody against osteopontin. Scale bar, 50 μm. (**f**) Different MSC loads detected in the tumours as demonstrated by the colony-formation assay. Primary tumours with or without pri-miR-126 ectopic expression were collected 10 days after implantation. GFP^- tumour-associated stromal cells were purified using FACS. The stromal cells were counted and plated in MesenCult (StemCell Technologies) for 14 days for the detection of mouse MSCs. CFU-F colonies as shown in the figure inset were then counted, and normalized to the total number of plated stromal cells. Data are presented as mean±s.d. from three independent experiments. (**g**) *Ccl5* mRNA expression is correlated with MSC presence in the tumours. *Ccl5* mRNA was measured by rtPCR and normalized to β-actin using RNA isolated from GFP^- stromal cells derived from 4T1-C- and 4T1-M-initiated tumours. The data presented are shown as mean±s.d. collected from three independent experiments. $^{**}P < 0.01$.

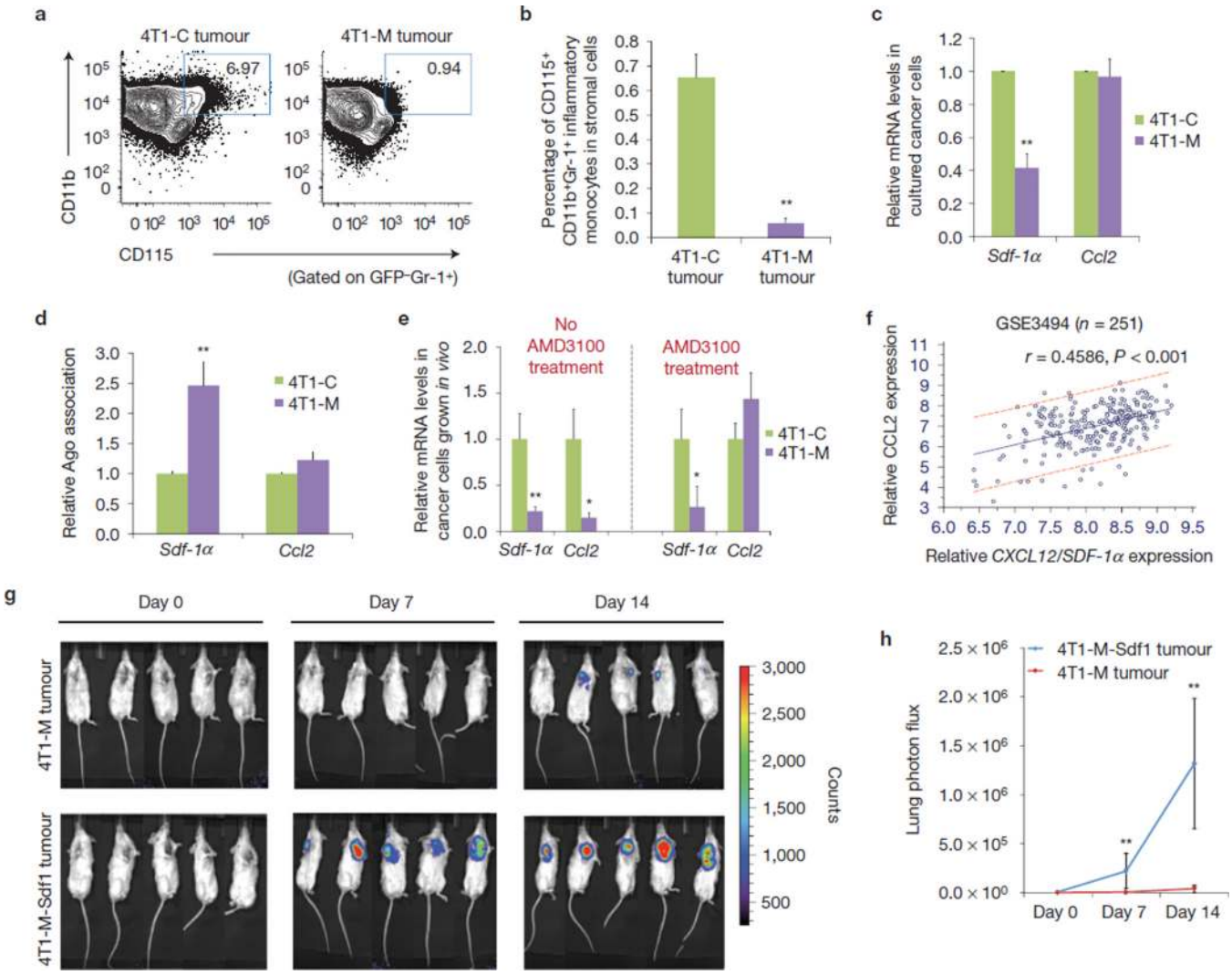

Figure 6.

miR-126/miR-126* regulate inflammatory monocyte recruitment through indirectly downregulating Ccl2 *in vivo*. (**a**) FACS analysis of tumours showing the proportion of $CD115^+CD11b^+Gr\text{-}1^+$ inflammatory monocytes inside the GFP^- tumour-associated stroma. (**b**) Quantification of the results shown in **a** for the percentage of $CD115^+CD11b^+Gr\text{-}1^+$ inflammatory monocytes in 4T1-C- and 4T1-M-initiated tumour stroma. The data presented are shown as mean±s.d. collected from three independent experiments. (**c**) *Sdf-1α* and *Ccl2* mRNA levels were measured by rtPCR and normalized to β-actin using RNA samples isolated from cultured 4T1-C and 4T1-M cells. The data presented are shown as mean±s.d. collected from three independent experiments. (**d**) The relative loading efficiency of *Sdf-1α* mRNA and *Ccl2* mRNA into RISC in 4T1-M versus 4T1-C cells. RISC-affiliated mRNAs were examined by quantitative rtPCR in the immunoprecipitates from 4T1-C or 4T1-M cells generated using an anti-Ago antibody, and normalized to expression levels in whole-cell lysates. The data presented are shown as mean±s.d. collected from three independent experiments. (**e**) Expression levels of *Sdf-1α* and *Ccl2* mRNA in GFP^+ 4T1-C or 4T1-M cells isolated from tumours were determined by rtPCR and normalized to β-actin as indicated. The procedure for AMD3100 treatment is described in Methods. The data presented are shown as mean±s.d. collected from three independent experiments. (**f**)

Correlation analysis between *SDF-1A* and *CCL2* expression profiles in breast cancer samples using the GSE3494 data set ($n = 251$). (**g**) Rescued Sdf-1α expression overcomes the suppressive effects of pri-miR-126 on the formation of lung metastases by 4T1-M cells. Approximately 5×10^4 4T1-M or 4T1-M-Sdf1 cells harbouring a luciferase reporter were inoculated into the mammary fat pad of 6-week-old female BALB/c mice as previously described. Primary tumours were surgically removed and metastatic lung lesion formation was monitored by the appearance of luciferase activity using imaging apparatus 7 and 14 days after primary tumour removal, $n = 5$ in each group. (**h**) Quantification of the results shown in **g**. The data presented are shown as mean±s.d. collected from five independent experiments. $^*P < 0.05$. $^{**}P < 0.01$.

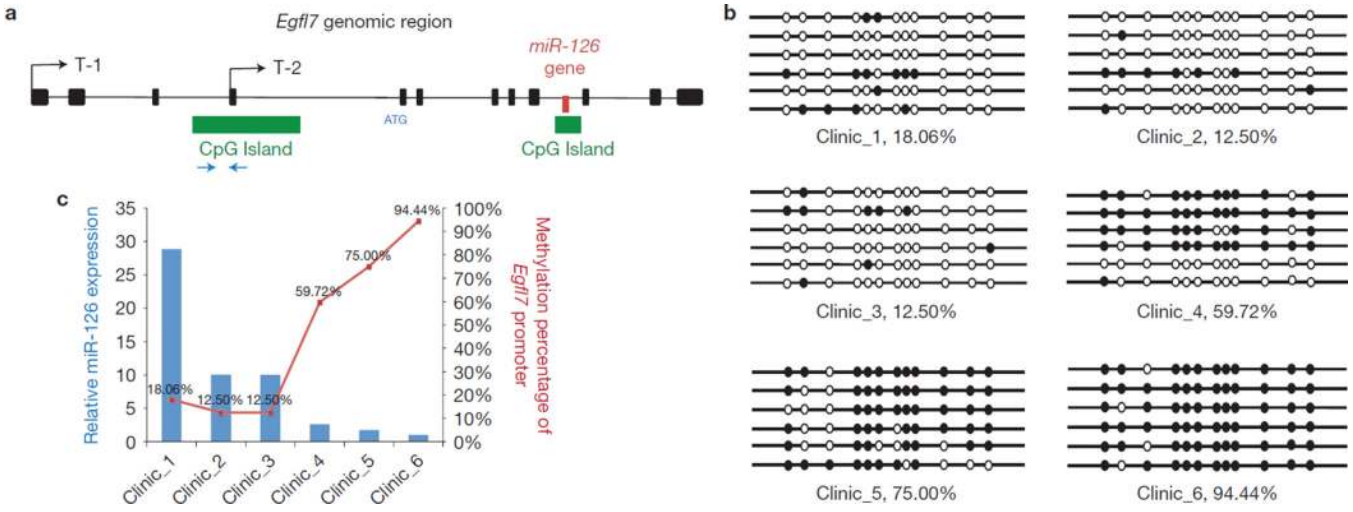

Figure 7.

Epigenetic regulation of miR-126 biogenesis through changes in the methylation status of the host gene *Egfl7* T2 promoter. (**a**) Schematic illustration of the location of the miR-126 gene inside an intron of *Egfl7*. Blue arrows indicate the region used for bisulphite genomic sequencing analysis. (**b**) Bisulphite genomic sequencing analysis of the CpG island of the *Egfl7* T-2 promoter in clinical breast tumour samples. Bisulphite sequencing PCR primers were designed using MethPrimer software, and a 205-nucleotide region containing 12 CpG islands was amplified after bisulphite conversion. The PCR products were then cloned into pCR^{TM}4 – TOPO TA vectors (Invitrogen). For each sample, six colonies were picked for sequencing and the indicated methylation percentage was calculated on the basis of the status of sequenced CpG islands. Black circles and open circles represent methylated and unmethylated CpG dinucleotides, respectively. (**c**) The miR-126 expression profile correlates with the methylation status of the *Egfl7* T2 promoter. miR-126 expression was determined by rtPCR and normalized to U6 RNA in these clinical samples. The methylation percentage was calculated using the bisulphite genomic sequencing results from **b**.